POLITECNICO DI TORINO
Repository ISTITUZIONALE

Experimental evaluation of mechanical properties repeatability of SLA polymers for labs-on-chip and bio-MEMS

(Article begins on next page)

19 April 2024

Experimental evaluation of mechanical properties repeatability of SLA polymers for labs-on-chip and bio-MEMS

Giorgio De Pasquale[1], Valentina Bertana[2], Luciano Scaltrito[2]

[1] Department of Mechanical and Aerospace Engineering, Politecnico di Torino, Italy
E-mail: giorgio.depasquale@polito.it

[2] Department of Applied Science and Technology, Politecnico di Torino, Italy

Abstract

Stereolithography (SLA) is a rapid prototyping technique based on photo-polymerization of liquid resin by laser source. The process is well known for many prototyping activities and additive manufacturing operations and started to show its potential in bio-MEMS applications like lab-on-chips. Unfortunately, the strong linkage between process parameters setting and final properties of downscaled devices is at present the primary cause of design failure and delays. In fact, it is crucial to control geometrical tolerances and mechanical properties. The aim of this work is to investigate the interactions between the most influent SLA process parameters on final mechanical and topological properties of biomedical polymers. The cross-interactions of polymer transparency, port-curing time and hatching direction are analyzed. The terms of comparison used to analyze process performances are geometrical dimensions and mechanical properties (Young's modulus, ultimate stress/strain). The analysis of variance (ANOVA) method is used to identify the factor of influence of each process parameter.

Keywords

Experimental mechanics, stereolithography, additive manufacturing, ANOVA, bio-MEMS, lab-on-chip.

1. Introduction

The large family of additive manufacturing (AM) techniques for polymers includes several methods for building components layer-by-layer, also called "layered manufacturing" or "solid freeform fabrication" (Richter and Jacobs 1991; Jacobs 1992; SFFPS 1993; Gurr and Mülhaupt 2012). These techniques include stereolithography (SLA), selective laser sintering (SLS) and fused deposition modeling (FDM). The stereolithographic process analyzed in this paper is based on the activation and solidification of liquid resin after laser exposure. The laser path is controlled to define the planar geometry of each polymer layer, having around 100μm thickness. After the activation and solidification of the exposed polymer surface, another layer of liquid resin is deposited over the solid part to start the new polymerization cycle. At the end of the process, the solid component is subjected

to UV light in the "post curing" process step for specific time in order to complete the polymerization of the internal unexposed regions.

The prediction and control of the mechanical properties of the final component is crucial for stable and reliable application of the SLA process in many fields such as structural engineering (Karalekas and Agelopoulos 2006), tissues engineering (Bose et al. 2013, Lantada et al. 2013), microfluidics (De Pasquale and Veijola 2008, De Pasquale 2013) and other biomedical fields (Melchels et al. 2010, De Pasquale 2015, De Pasquale et al. 2016, De Pasquale 2016). Mechanical and dimensional properties are influenced by the main process parameters of SLA: laser specifications (power, speed, spot size, etc.), resin chemical properties and polymerization mechanism (Dulieu-Barton et al. 2000). Several studies have been conducted to investigate the influence of SLA process parameters on final properties, for instance by investigating the final strength of components (Chockalingam et al. 2008) and parts shrinkage (Wang et al. 1996). Different process parameters have been considered in analyzing process performances, including post curing time (Zhou et al. 2000, Nee et al. 2001, Salmoria et al. 2009). In some cases, advanced methodological methods have been applied as accuracy models (Lynn-Charney et al. 2000) and genetic algorithms (Cho et al. 2000).

Labs-on-chip are usually identified as integrated biological sensors, but can be considered more generally as an environment for the electrical detection of biological elements. They are used as optical, micromechanical, electrical, chemical, piezoelectric or thermal transducers to detect physical samples properties in small areas (Lafleur et al. 2016). The application of additive manufacturing processes to fabricate labs-on-chip and fluidic bio-MEMS (micro electro-mechanical systems) is at the first steps. However it is opening to innovative potentialities and performances (Andrè 2017) of the devices, such as increased geometrical complexity, flexibility, and improved materials variability. The main challenges in fabricating fluidic sensors are related to the stringent requirements about dimensional tolerances and mechanical properties stability. On the other hand, 3D printing of polymers with SLA at the microscale for MEMS applications is very promising for many reasons: a) the microfabrication chain is dramatically simplified in comparison with IC-derived processes (including lithography, deposition, etching, baking, etc.), b) sophisticated and expensive facilities, including cleanrooms, are not required, c) high speed and high volumes of production can be achieved, d) additional materials different from traditional metals and silicon can be used.

Additive manufacturing of polymers through SLA was originally developed for rapid prototyping in the millimeter scale; the downscaling process requires to know more in detail how to control and predict dimensional tolerances and mechanical properties of devices by modifying the main process parameters. After defining the laser setup, which is treated as machine-related property, the SLA process is subjected to operative variables associated to the direction of hatching with respect to the direction of load, the post curing time and the optical properties of the polymer used (i.e. the polymer transparency). Previous studies in the macroscale demonstrated the influence and cross-talk of these parameters on final results of SLA process (Chockalingam et al. 2008, Wang et al. 1996, Zhou et al. 2000, Nee et al. 2001, Salmoria et al. 2009).

This paper reports the experimental evaluation of the factor of influence of the three mentioned operational SLA process parameters on final dimensional and mechanical properties of the device. Dedicated samples for tensile tests have been fabricated and analyzed according to ANOVA technique. The process performances variability is evaluated in terms of in-plane and out-of-plane

dimensional tolerances, material properties (Young's modulus) and mechanical response (ultimate stress and strain).

2. The SLA process in bio-MEMS

The Microla Optoelectronics SLA machine (Ventola et al. 2014, Chen et al. 2010) is used for samples fabrication. It has 200x170mm^2 working area and it is equipped by 405nm laser source.

The process sequence applied to samples fabrication is described by the following steps: 1) the machine tank is filled with liquid resin; 2) the laser produces the polymerization of the superficial resin layer (about 100µm thick) under controlled path; 3) the machine stage moves downwards until the top layer is covered by flowing liquid resin, then the process restarts from point 2; 4) when the component is completed, isopropyl alcohol is applied to remove resin residues; 5) the post-curing treatment, based on UV exposure for given time, is applied to complete the polymerization of those regions previously remained unexposed.

The application of SLA process to the fabrication of bio-MEMS, fluidic devices and labs-on-chip is opening to innovative properties and performances such as freedom of shape and flexibility. Then, the fabrication of curved surfaces and devices having high number of layers is feasible with SLA, while it is not possible with common micromachining techniques. Materials compatible with human body are available with SLA instead of traditional metals and silicon applied to MEMS microfabrication; finally, aspect ratios higher than those of LIGA processes can be achieved (Andrè 2017, Varadan and Varadan 2001, Ratchev and Koelemeijer 2008, Bhushan and Caspers 2017).

The SLA machine was calibrated before the use. Since the efficiency of the process is strictly related to the correct polymerization of the liquid resin, the attention was put on laser power and laser focusing/spot dimension.
As regards the latter, the Beam Profiler Spiricon SP503U was used to set the focus point. By positioning the instrument on the printer platform and making the laser beam enter in the instrument objective, it was possible to observe the beam intensity profile and the spot diameter. For a Gaussian beam, the beam radius is found as the distance from the beam axis where the intensity drops to $1/e^2$. The focus point of a Gaussian beam can be defined as the distance from the laser source where the beam changes from convergent to divergent propagation passing through a plane of minimum radius. Considering this, the focus point was found moving the platform along the z-axis until the minimum diameter was read.
Afterwards, the laser power was checked by setting a value from the machine software (from 10mW to 120mW by 10mW steps) and measuring the beam power with the power meter STANDA 11UP25-H. This check confirmed a correct setting of the laser power by the control board mounted in the SLA machine.

3. Experimental analysis

The reported experimental analysis consists of tensile tests of dedicated samples built with controlled fabrication parameters combinations. The setup of parameters values and their cross-interactions are influencing the dimensional accuracy and mechanical properties of microstructures and labs-on-chip. The factors of influence of three operative process parameters on the final samples properties are evaluated with ANOVA. The resin FTD-SB (on-line reference) used for samples fabrication through

SLA process is composed by acrylate monomers, glycol diacrylate monomers and phosphine oxide based photo initiator. It is characterized by nominal 100cp viscosity, 35 shore D hardness, and 1016 g/dm^3 density.

3.1. Samples design and fabrication

Samples are designed according to the ISO527 (and ASTM D638) standard about experimental characterization of mechanical properties of materials. The shape and dimensions of samples are reported in Fig. 1a. The length of the central region (i.e. gauge region) is higher than shoulders width to prevent notch effects. Additionally, in the gauge region, the length must be at least four times the width according to standard requirements. After fabrication process, each sample has been numbered. Initial values of process parameters have been set according to Cho et al. 2000, which reports the fabrication of components with comparable features: 100μm layer thickness, 50μm hatch spacing (i.e. the distance between adjacent laser trajectories). The other fixed parameters of the process are: 30mW laser power, 1000mm/s laser hatching velocity in edges, 2000mm/s laser hatching velocity in internal areas, 120W ultraviolet source power for post curing process.

3.2. Design of experiments

According to the DOE technique, the following operative process parameters are considered: 1) laser hatching direction, 2) post-curing time and 3) polymer transparency. Laser hatching direction determines the orientation of polymerized regions of the resin, which can be ideally associated to solid stripes aligned together and joined by underexposed polymer with lower strength. Indeed, post-curing process has the goal to complete the polymerization of the unexposed regions. This polymerization is proportional to the post-curing duration. Finally, polymer transparency is an indicator of the optical properties of the resin and of the penetration of laser light beam inside the material: high transparency means deep penetration of light and faster polymerization.

Two levels (or variants) per parameter are considered. The laser hatching direction of polymerization is varied along x and y axes, respectively parallel and orthogonal to tensile load direction (Fig. 1b). Post-curing time levels are 14 and 60min (including both sample sides, each one exposed respectively for 7 and 30min in the two cases). The polymer transparency levels are low (i.e. opaque polymer) and high (i.e. clear polymer), depending on different additives inside the resin. The arrangement of different parameter values produces the 8 combinations reported in Tab.1, which are used to fabricate 40 samples (5 identical samples per combination). Samples 6-10 (opaque) and 21-25 (clear) are reported in Figs. 2a and 2b as an example.
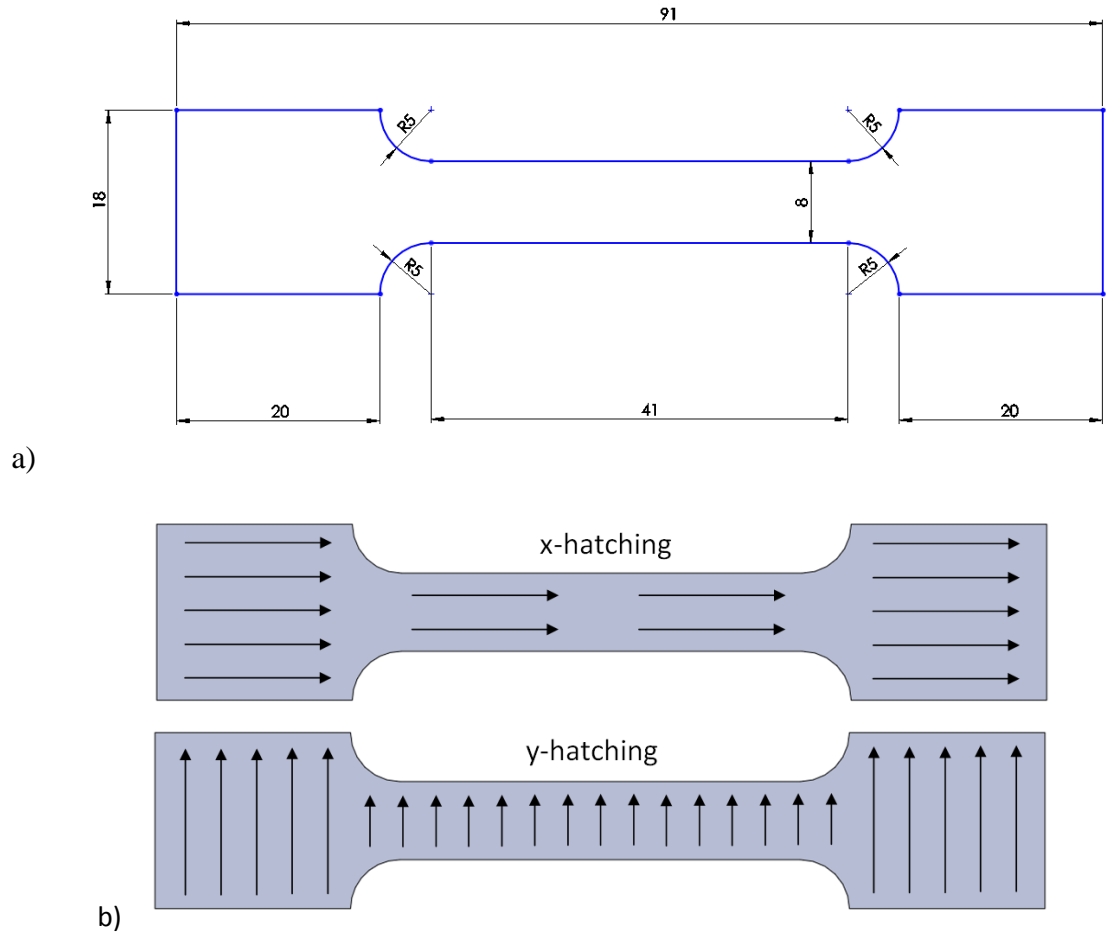
a)

b)

Fig. 1. Nominal dimensions (in millimeters) of the tensile test sample (thickness is 4 mm) (a),
qualitative representation of hatching direction along x and y axes (b).

Table 1. Samples numbering and description of technological parameters combinations.

Samples	Hatching direction	Post curing time (min)	Polymer transparency	Parameters combination
1-5	x	14	Opaque	1
6-10	x	60	Opaque	3
11-15	y	60	Opaque	4
16-20	y	14	Opaque	2
21-25	x	60	Clear	7
26-30	x	14	Clear	5
31-35	y	14	Clear	6
36-40	y	60	Clear	8
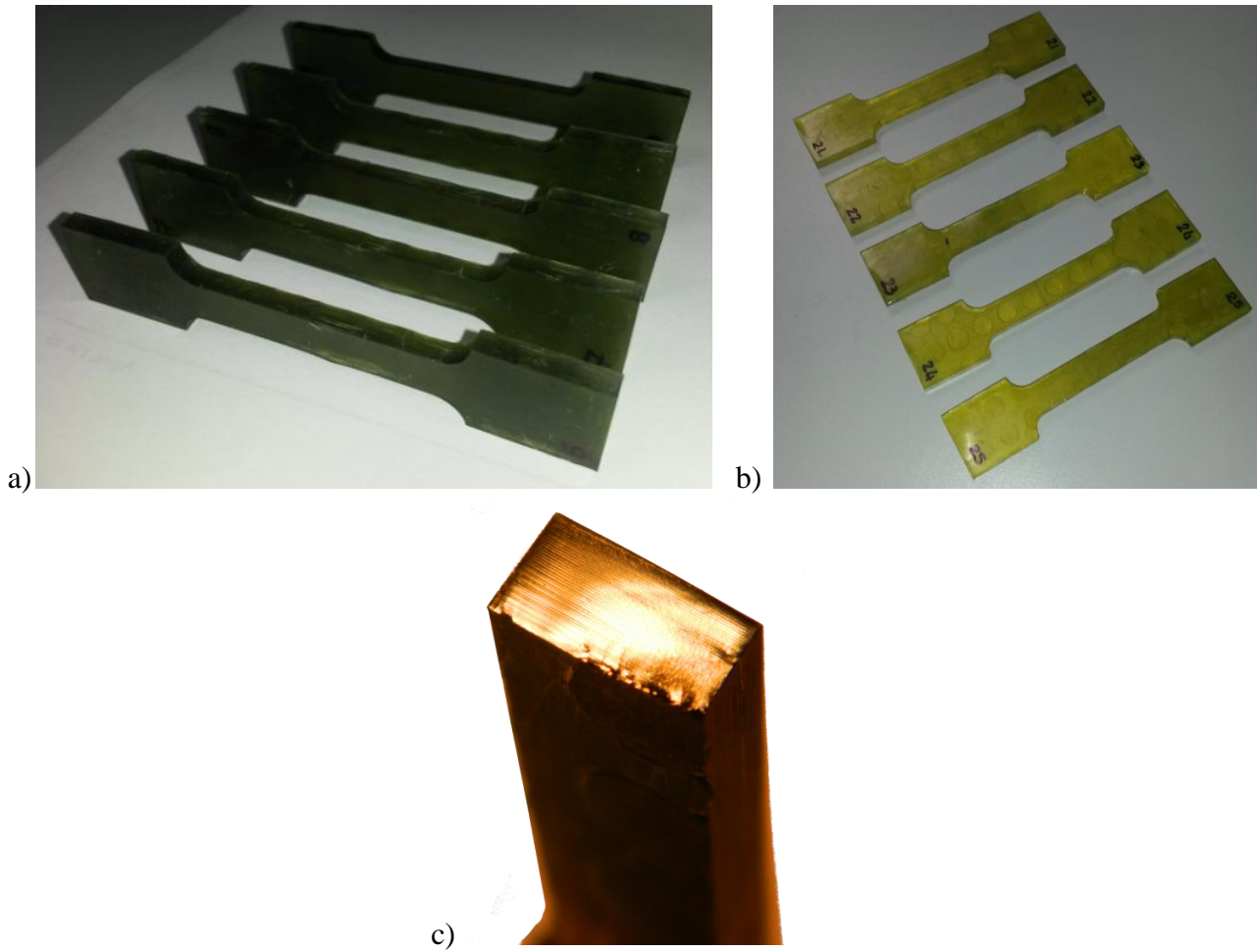
Fig. 2. Samples 6-10 (opaque) (a) and 21-25 (clear) (b) and fracture surface (c).

3.3. Dimensional characterization

Samples dimensions and geometry are measured by means of the micrometer gauge (Mitutoyo, range 0-25mm, resolution 0.01mm). 10 representative dimensions represented are used to detect the most frequent errors of accuracy and repeatability associated to the process. These dimensions include sample widths and thicknesses at different axial positions, also in correspondence of shoulders (the clamping zone) and gauge area (the central part of the sample).

3.4. Mechanical properties characterization

The force-displacement curve of each sample is measured with the standard electro-mechanical tensile testing machine MTS Q Test 10 (10kN max capacity, 1016mm max travel). Tensile tests are conducted at imposed displacement with 0.5mm/min velocity at room temperature (25°C) by 10kN load cell.

4. Results

4.1. Dimensions and geometry

The dimensional measurement obtained on each sample are reported in the Appendix and their mean, standard deviation and variance are reported in Tabs. 2 and 3.

Table 2. Mean, standard deviation and variance among dimensional measurements of samples 1-20 (opaque).

			X hatching direction		Y hatching direction	
			Post curing time		Post curing time	
		Unit	14 min	60 min	14 min	60 min
Thickness (S_i)	Mean (μ)	mm	4.31	4.41	4.64	4.60
	St. Dev. (σ)	mm	0.21	0.19	0.22	0.15
	Variance (σ^2)	mm^2	0.044	0.037	0.047	0.023
Shoulder widths (L_a, L_b)	Mean (μ)	mm	17.57	17.64	17.56	17.59
	St. Dev. (σ)	mm	0.04	0.04	0.05	0.06
	Variance (σ^2)	mm^2	0.001	0.001	0.002	0.004
Gauge widths (L_m, L_{ma}, L_{mb})	Mean (μ)	mm	7.94	7.94	7.90	7.89
	St. Dev. (σ)	mm	0.04	0.03	0.04	0.06
	Variance (σ^2)	mm^2	0.001	0.001	0.002	0.003

Table 3. Mean, standard deviation and variance among dimensional measurements of samples 21-40 (clear).

			X hatching direction		Y hatching direction	
			Post curing time		Post curing time	
		Unit	14 min	60 min	14 min	60 min
Thickness (S_i)	Mean (μ)	mm	4.44	4.56	4.47	4.58
	St. Dev. (σ)	mm	0.19	0.30	0.31	0.32
	Variance (σ^2)	mm^2	0.037	0.093	0.099	0.101
Shoulder widths (L_a, L_b)	Mean (μ)	mm	17.84	17.79	17.81	17.75
	St. Dev. (σ)	mm	0.03	0.04	0.02	0.03
	Variance (σ^2)	mm^2	0.001	0.002	0.001	0.001
Gauge widths (L_m, L_{ma}, L_{mb})	Mean (μ)	mm	8.07	8.05	8.07	8.04
	St. Dev. (σ)	mm	0.03	0.02	0.02	0.01
	Variance (σ^2)	mm^2	0.001	$3.1 \cdot 10^{-4}$	$3.4 \cdot 10^{-4}$	$2.1 \cdot 10^{-4}$

4.2. Mechanical properties

The stress-strain curves of samples 16-20 and 31-35 are reported in Fig. 3 as an example of static material behavior. All samples show brittle fracture and some variation of material strength between clear and opaque polymers is visible (ultimate stress and ultimate strain increase up to 45% and 50% respectively for clear polymer). The detail of the brittle fracture surface after the tensile test is reported in Fig. 2c. The experimental results of samples mechanical characterization is reported in the

Appendix, where E is the Young's modulus, σ_r is the ultimate stress, ε_{tot} is the total strain, composed by the linear and nonlinear contributions (ε_{lin} and ε_{nonlin}), and ΔL_r is the ultimate elongation. Mean, standard deviation and variance values are listed in Tabs. 4 and 5.
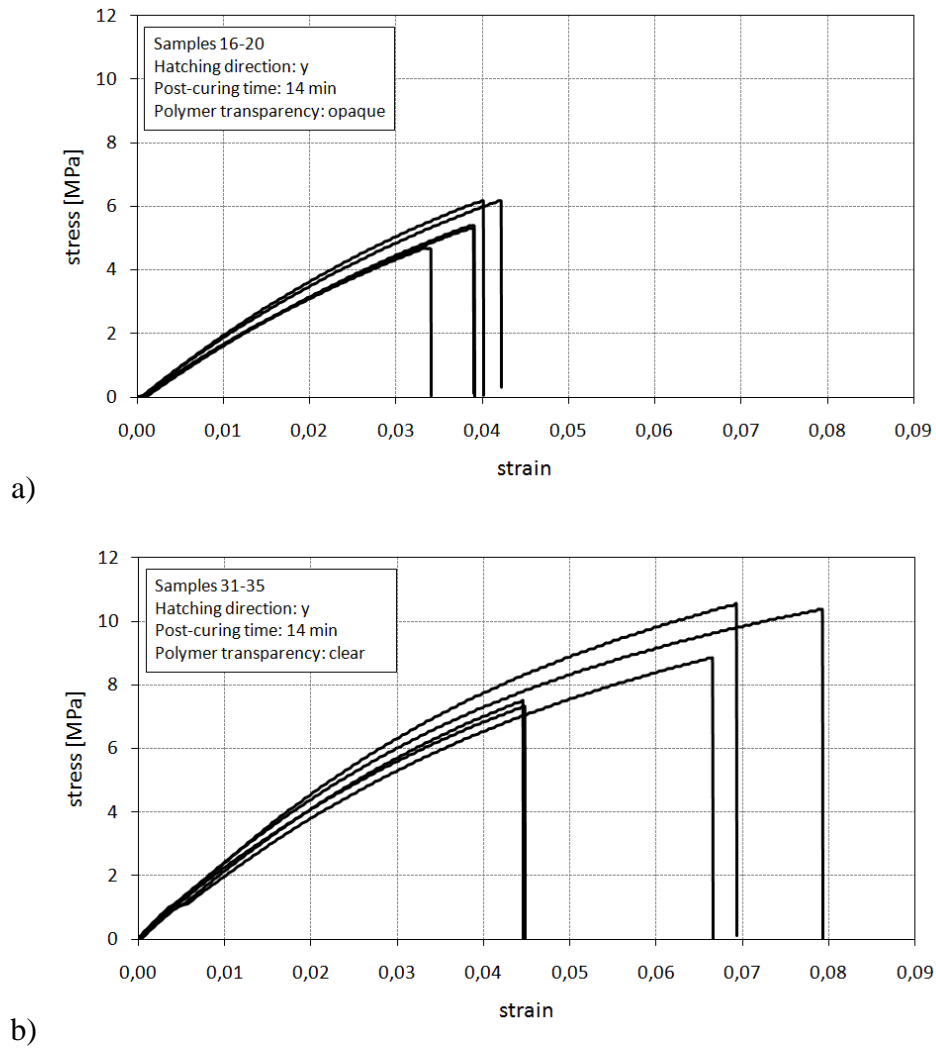

a)

b)

Fig. 3. Variation of mechanical strength in case of opaque and clear polymers as evidences of samples 16-20 (a) and 31-35 (b) respectively.

Table 4. Mean, standard deviation and variance of mechanical characterization of samples 1-20 (opaque).

		Unit	Mean (μ)	St. Dev. (σ)	Variance (σ²)
Samples 1-5 x-hatching PCT 14 min	E	MPa	223.08	17.73	314.21
	σ_r	MPa	7.08	1.86	3.47
	ε_{tot}	-	0.050	0.017	$2.85 \cdot 10^{-4}$
	ΔL_r	mm	0.99	0.59	0.35
Samples 6-10 x-hatching	E	MPa	244.76	25.26	638.18
	σ_r	MPa	8.69	0.96	0.92

PCT 60 min	ε_{tot}	-	0.058	0.011	$1.27 \cdot 10^{-4}$
	ΔL_r	mm	1.13	0.34	0.12
Samples 11-15 y-hatching PCT 60 min	E	MPa	271.15	16.30	265.70
	σ_r	MPa	7.16	0.54	0.29
	ε_{tot}	-	0.040	0.005	$2.98 \cdot 10^{-5}$
	ΔL_r	mm	0.68	0.16	0.03
Samples 16-20 y-hatching PCT 14 min	E	MPa	197.89	13.75	189.04
	σ_r	MPa	5.56	0.57	0.32
	ε_{tot}	-	0.038	0.003	$8.96 \cdot 10^{-6}$
	ΔL_r	mm	0.52	0.07	0.01

Table 5. Mean, standard deviation and variance of mechanical characterization of samples 21-40 (clear).

		Unit	Mean (μ)	St. Dev. (σ)	Variance (σ^2)
Samples 21-25 x-hatching PCT 60 min	E	MPa	306.07	29.68	881.04
	σ_r	MPa	8.86	1.03	1.06
	ε_{tot}	-	0.045	0.008	$6.90 \cdot 10^{-5}$
	ΔL_r	mm	0.80	0.33	0.11
Samples 26-30 x-hatching PCT 14 min	E	MPa	243.77	29.28	857.24
	σ_r	MPa	8.85	1.32	1.75
	ε_{tot}	-	0.057	0.009	$8.02 \cdot 10^{-5}$
	ΔL_r	mm	1.06	0.38	0.14
Samples 31-35 y-hatching PCT 14 min	E	MPa	258.36	32.82	1077.26
	σ_r	MPa	8.93	1.36	1.85
	ε_{tot}	-	0.061	0.014	$1.94 \cdot 10^{-4}$
	ΔL_r	mm	1.33	0.59	0.35
Samples 36-40 y-hatching PCT 60 min	E	MPa	325.76	25.79	665.10
	σ_r	MPa	8.38	1.55	2.39
	ε_{tot}	-	0.039	0.009	$8.80 \cdot 10^{-5}$
	ΔL_r	mm	0.68	0.32	0.10

4.3. Factors of influence

The factor of influence of each operative process parameter considered on dimensional and material properties of samples is calculated by using ANOVA method. More specifically, the influence of the value (or level) of each process parameter on the experimental results previously reported is calculated, as reported in Table 6. The experimental data considered are referred to the dimensions (thickness and shoulder width) and material properties (Young's modulus, ultimate stress and total strain) of samples. For example, the influence of x/y hatching directions on the variance of experimental detections is calculated by fixing the other two process parameters (e.g. post-curing time = 14 min and polymer transparency = clear for the first row of Tab. 6). The ANOVA is applied to two populations of 5 identical samples, which only differs for the desired process parameter level considered. In the first case described, the parameters combination considered are the numbers 5 and

6, corresponding to sample groups 26-30 and 31-35 respectively (Tab. 1). Then, the same calculation is repeated for every values/levels combination of the fixed process parameters.

The variance among each group of samples is calculated as

$$s_a^2 = \frac{n_k}{a-1} \sum_{k=1}^{a} \left(\bar{X}_k - \bar{X} \right)^2 \tag{1}$$

with (a-1) degrees of freedom, where k is the group number, n_k is the number of samples in group k, $\bar{X}_k$ is the mean of group k, and $\bar{X}$ is the general mean of all groups. The variance inside groups is calculated as

$$s_i^2 = \frac{\sum\limits_{k=1}^{a} D_k}{\sum\limits_{k=1}^{a} (n_k - 1)} \tag{2}$$

with $\sum\limits_{k=1}^{a} (n_k - 1)$ degrees of freedom, where D_k is the deviance inside group k. Finally, the factor of influence is calculated as

$$F = \frac{s_a^2}{s_i^2} \tag{3}$$

Figure 4 reports the values of the factor of influence for each parameters combination, with reference to the experimental dimensions and mechanical properties considered.

Table 1. Parameters combinations and related samples used to evaluate factors of influence.

		Fixed values						Parameters combination	Samples
		Hatching direction		P.C. time		Transparency			
		x	y	14 min	60 min	opaque	clear		
Factor of influence	Hatching direction	/		X			X	5-6	26-30/31-35
					X		X	7-8	21-25/36-40
				X		X		1-2	1-5/16-20
					X	X		3-4	6-10/11-15
	P.C. time	X		/		X		1-3	1-5/6-10
			X			X		2-4	16-20/11-15
		X					X	5-7	26-30/21-25
			X				X	6-8	31-35/36-40
	Transparency	X		X		/		1-5	1-5-/26-30
			X	X				2-6	16-20/31-35
		X			X			2-7	16-20/21-25
			X		X			4-8	11-25/36-40
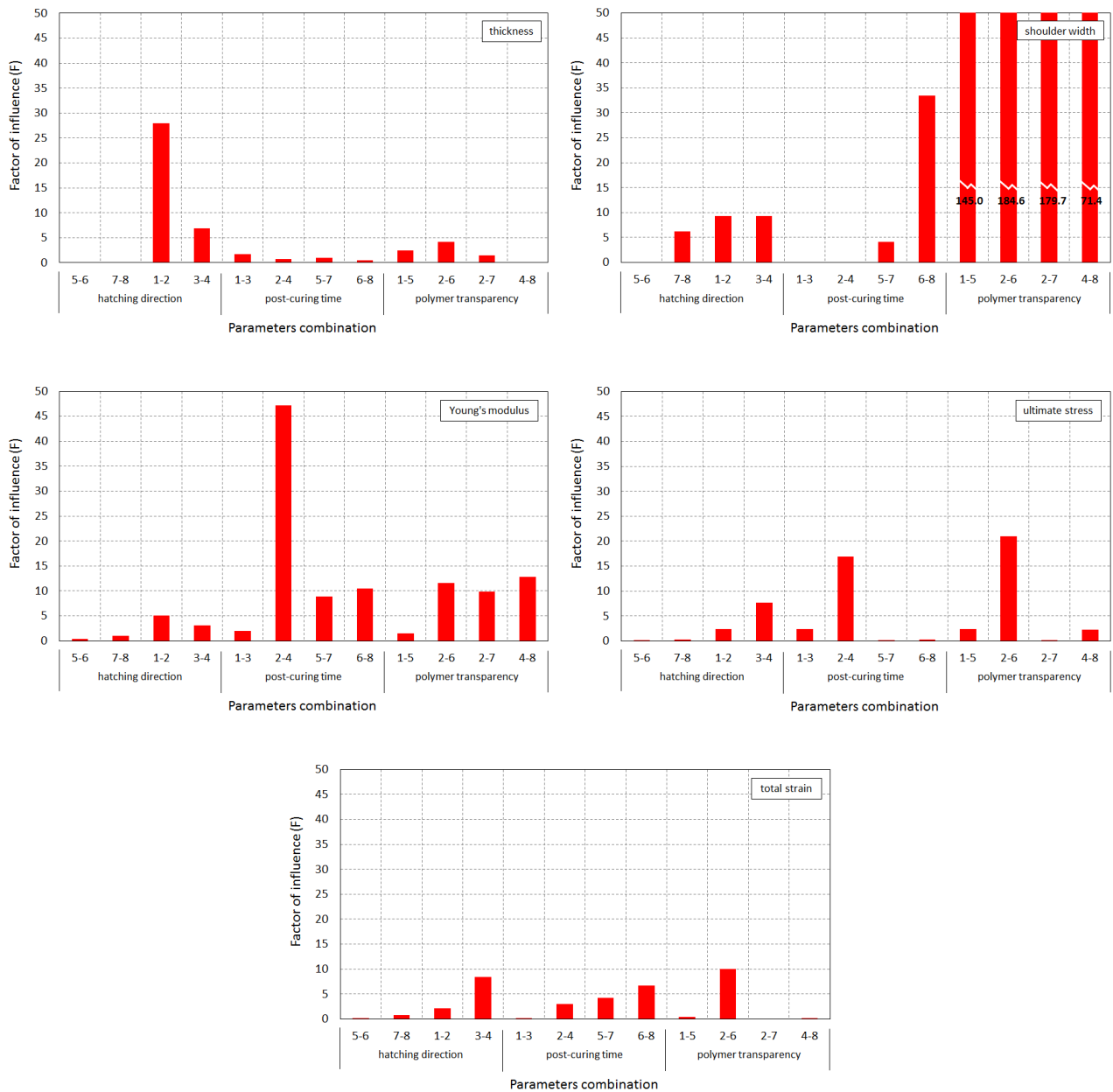
Figure 4. Factor of influence of each parameters combination considered with reference to Tab. 1 with respect to geometrical (thickness, shoulder width) and material (Young's modulus, ultimate stress, total strain) properties.

5. Discussions

The result of dimensional measurements reported in Tab. 3 reveals that the real thickness is always higher than the corresponding nominal value, independently to resin typology and other operative process parameters. Clear samples (0-20) show in average shoulder and gauge widths higher than opaque samples (21-40); opaque samples also have widths lower than the corresponding nominal values. Only for opaque samples, the hatching direction along x-axis is associated to higher accuracy of dimensions; however, the same relation is not present in clear samples. About mechanical

properties, all samples show brittle behavior independently to the resin type and process parameters. This is testified by the stress-strain curve shape and orientation of fracture surface with respect to sample axis (about 90°) reported in Fig. 2c.

The analysis of operative process parameters reported in Fig. 4, indicates that the polymer transparency has dramatically high influence on the in-plane geometrical dimensions ($F=145$ in average with all combinations of other two process parameters) and moderate influence on the Young's module ($F=8.9$), while it has not appreciable influence on out-of-plane dimensions (or thickness) and total strain ($F=2.0$ and 2.6 respectively). The influence of transparency is very low also on the ultimate stress ($F=1.5$), except when 14min post-curing time and y hatching directions are present (combination 2-6, with $F=21.0$).

About post-curing time, the effect of this parameter is generally low ($F=2.1$), except for few specific combination of parameters: 2-4 on the Young's modulus ($F=47.2$) and ultimate stress ($F=16.9$), 5-7 on the Young's modulus ($F=8.9$) and 6-8 on shoulder width ($F=33.4$) and Young's modulus ($F=10.4$).

Hatching direction has moderate influence on geometrical dimensions ($F=8.7$ and 6.22 in average for thickness and width respectively), and low influence on material properties ($F=2.4$, 2.6 and 2.9 in average for Young's modulus, ultimate stress and total strain respectively).

6. Conclusions

The validation of SLA process demonstrates the influence of some selected parameters on the final geometrical accuracy and mechanical strength of the acrylic polymer usable for fluidic devices and labs-on-chip. In particular, the polymer transparency deeply affects the in-plane geometrical tolerances of components; this is due to the alteration of laser beam paths inside the material caused by variable diffraction angles in case of different degree of resin transparency. This effect is accentuated at the sample edges, where altered light paths modified the extension of the exposed region and produces significant differences in final dimensions. Geometrical tolerances (in-plane and out-of-plane) are then affected by hatching direction, although more slightly than by transparency. Mechanical properties feel the moderate influence of polymer transparency and post-curing time (especially about Young's modulus and, with particular process setup combinations, about ultimate stress), which are directly related to the percentage of polymerization of the resin.

Appendix

Experimental measurements on samples and nominal values (dimensions in millimeters).

Sample	S_{ad}	S_{ac}	S_{mc}	S_{bc}	S_{bd}	L_a	L_{ma}	L_m	L_{mb}	L_b
1	4.40	4.46	3.84	3.95	4.02	17.56	7.94	8.02	7.92	17.57
2	4.46	4.35	4.32	4.67	4.59	17.52	7.89	7.95	7.91	17.55
3	4.29	4.39	4.17	4.26	4.37	17.61	7.92	7.94	7.94	17.57
4	4.45	4.68	4.35	4.45	4.29	17.54	8.00	7.93	7.89	17.56
5	4.14	4.40	4.17	4.27	3.96	17.59	7.94	7.97	7.99	17.66
6	4.35	4.46	4.31	4.66	4.56	17.61	7.95	7.94	7.91	17.61
7	4.16	4.33	4.17	4.71	4.36	17.73	8.00	8.00	7.97	17.67

8	4.53	4.77	4.31	4.61	4.35	17.63	7.95	7.95	7.93	17.61
9	4.40	4.30	4.32	4.69	4.59	17.62	7.93	7.93	7.93	17.63
10	4.11	4.60	4.23	4.41	4.06	17.63	7.93	7.92	7.93	17.62
11	4.78	4.72	4.61	4.67	4.45	17.47	7.78	7.87	7.88	17.57
12	4.48	4.64	4.67	4.70	4.72	17.55	7.82	7.86	7.90	17.57
13	4.28	4.60	4.53	4.70	4.77	17.66	7.83	7.96	7.95	17.66
14	4.28	4.59	4.54	4.74	4.77	17.55	7.90	7.92	7.91	17.57
15	4.77	4.67	4.37	4.50	4.35	17.68	7.96	7.97	7.84	17.66
16	4.41	4.59	4.52	4.67	4.66	17.57	7.92	7.93	7.94	17.56
17	4.60	4.75	4.36	4.52	4.30	17.64	7.97	7.95	7.84	17.64
18	4.68	4.85	4.48	4.58	4.32	17.51	7.86	7.86	7.90	17.59
19	4.83	4.67	4.98	4.52	4.34	17.52	7.91	7.92	7.79	17.52
20	4.46	4.88	4.86	5.10	4.96	17.57	7.89	7.88	7.90	17.52
21	4.47	4.88	4.19	4.87	4.23	17.76	8.05	8.07	8.04	17.75
22	4.28	4.55	4.23	4.63	4.45	17.77	8.04	8.03	8.02	17.77
23	4.83	4.75	4.35	4.89	4.90	17.77	8.05	8.08	8.06	17.82
24	4.30	4.28	4.04	4.95	4.31	17.85	8.05	8.08	8.07	17.87
25	4.55	4.58	4.35	4.80	5.30	17.76	8.06	8.06	8.03	17.78
26	4.44	4.46	4.02	4.34	4.34	17.87	8.09	8.09	8.06	17.85
27	4.59	4.64	4.20	4.51	4.52	17.80	8.04	8.03	8.04	17.83
28	4.37	4.94	4.15	4.52	4.35	17.82	8.04	8.08	8.07	17.87
29	4.34	4.71	4.34	4.75	4.34	17.83	8.07	8.04	8.03	17.83
30	4.58	4.41	4.39	4.45	4.31	17.83	8.10	8.12	8.10	17.89
31	4.84	4.83	4.15	4.34	4.06	17.80	8.10	8.10	8.08	17.85
32	4.90	4.87	4.35	4.33	4.02	17.76	8.06	8.07	8.05	17.80
33	4.29	4.49	4.26	5.02	4.98	17.83	8.07	8.09	8.07	17.80
34	4.00	4.36	4.23	4.73	4.74	17.83	8.07	8.07	8.06	17.80
35	4.72	4.60	4.23	4.36	4.13	17.82	8.04	8.05	8.04	17.79
36	4.95	4.95	4.27	4.35	4.34	17.69	8.02	8.02	8.03	17.75
37	5.08	5.02	4.33	4.61	4.44	17.70	8.03	8.06	8.05	17.76
38	4.84	4.85	4.14	4.27	4.20	17.77	8.03	8.04	8.03	17.78
39	4.91	4.84	4.22	4.41	4.34	17.71	8.03	8.02	8.02	17.79
40	5.05	5.04	4.35	4.48	4.34	17.75	8.04	8.06	8.06	17.75
Nominal value	4.00	4.00	4.00	4.00	4.00	18.00	8.00	8.00	8.00	18.00

Experimental results of mechanical characterization of samples.

Sample	E [MPa]	σ_r [MPa]	ε_{tot}	ε_{lin}	ε_{nonlin}	ΔL_r [mm]
1	257.95	10.57	0.082	0.041	0.041	2.11
2	217.10	7.34	0.054	0.034	0.020	1.01
3	217.55	6.15	0.043	0.028	0.015	0.74
4	214.27	6.05	0.037	0.028	0.009	0.47
5	208.54	5.29	0.037	0.025	0.012	0.61
6	258.25	8.29	0.047	0.032	0.015	0.75
7	219.54	7.03	0.048	0.032	0.016	0.80
8	274.09	8.98	0.054	0.033	0.021	1.09

9	262.00	9.71	0.064	0.037	0.027	1.38
10	209.90	9.43	0.077	0.045	0.032	1.64
11	278.93	7.92	0.042	0.028	0.014	0.70
12	295.33	6.85	0.032	0.023	0.009	0.47
13	272.42	6.91	0.036	0.025	0.010	0.52
14	246.50	7.65	0.048	0.031	0.017	0.85
15	262.56	6.49	0.041	0.025	0.017	0.86
16	204.71	6.19	0.042	0.030	0.012	0.59
17	187.66	4.68	0.033	0.025	0.009	0.44
18	221.23	6.18	0.040	0.028	0.012	0.60
19	182.86	5.42	0.038	0.030	0.009	0.44
20	193.01	5.32	0.038	0.028	0.011	0.56
21	329.38	10.65	0.058	0.032	0.025	1.28
22	263.72	7.57	0.035	0.029	0.006	0.33
23	337.69	8.35	0.041	0.025	0.016	0.84
24	277.53	8.59	0.050	0.031	0.019	0.98
25	322.02	9.13	0.039	0.028	0.011	0.56
26	195.75	6.76	0.046	0.035	0.012	0.59
27	240.29	8.14	0.049	0.034	0.015	0.76
28	240.13	9.08	0.071	0.038	0.033	1.69
29	256.59	9.61	0.061	0.037	0.023	1.19
30	286.08	10.66	0.059	0.037	0.021	1.08
31	252.74	7.52	0.044	0.030	0.015	0.74
32	302.56	10.37	0.079	0.034	0.045	2.30
33	286.53	10.57	0.069	0.037	0.032	1.65
34	211.19	8.87	0.067	0.042	0.025	1.25
35	238.80	7.35	0.045	0.031	0.014	0.72
36	295.31	6.66	0.029	0.023	0.007	0.34
37	330.89	7.62	0.030	0.023	0.007	0.36
38	305.69	7.28	0.036	0.024	0.012	0.62
39	370.12	9.58	0.048	0.026	0.022	1.12
40	326.77	10.77	0.052	0.033	0.019	0.98

References

André JC (2017) From Additive Manufacturing to 3D/4D Printing 1: From Concepts to Achievements. Wiley-ISTE.

André JC (2017) From Additive Manufacturing to 3D/4D Printing 2: Current Techniques, Improvements and their Limitations. Wiley-ISTE.

André JC (2017) From Additive Manufacturing to 3D/4D Printing 3: Breakthrough Innovations: Programmable Material, 4D Printing and Bio-printing. Wiley-ISTE.

Bose S, Vahabzadeh S, Bandyopadhyay A (2013) Bone tissue engineering using 3D printing. Materials Today, 16(12):496-504.

Bhushan B, Caspers M (2017) An overview of additive manufacturing (3D printing) for microfabrication. Microsyst Technol 23:1117-1124.

Chen Q, Chen Q, Maccioni G, Ferrero S, Scaltrito L, Sacco A (2010) Fabrication of micro-structures on Nickel alloy by DPSS laser ablation technique for lab-on-chip applications Proc. of SPIE, The International Society For Optical Engineering, 7762:776239.

Cho HS, Park WS, Choi BW, Leu MC (2000) Determining optimal parameters for stereolithographic processes via genetic algorithm. J Manuf Syst 19(1):18-27.

Chockalingam K, Jawahar N, Chandrasekar U, Ramanathan KN (2008) Establishment of process model for part strength in stereolithography. J Mater Process Tech 208:348-365.

De Pasquale G (2013) Experimental analysis of viscous and material damping in microstructures through the interferometric microscopy technique with climatic chamber. J Sound Vib 332:4103-4121.

De Pasquale G (2015) Biomechanical energy harvesting: design, testing, and future trends in healthcare and human-machines interfacing, In: "Innovative materials and systems for energy harvesting applications", L. Mescia, O. Losito, F. Prudenzano, IGI Global - Engineering Science Reference, USA, 290-340.

De Pasquale G (2016) Artificial human joint for the characterization of piezoelectric transducers in self-powered telemedicine applications. Meccanica, 51(9):2259-2275.

De Pasquale G, Kim SG, De Pasquale D (2016) GoldFinger: wireless human–machine interface with dedicated software and biomechanical energy harvesting system. IEEE-ASME T Mech 21(1):565-575.

De Pasquale G, Veijola T (2008) Comparative numerical study of FEM methods solving gas damping in perforated MEMS devices. Microfluid Nanofluid 5: 517-528.

Dulieu-Barton JM, Fulton MC (2000) Mechanical properties of a typical stereolithography resin. Strain, 36(2):81-87.

Gurr M, Mülhaupt R (2012) Rapid prototyping, in "Polymer Science: A comprehensive Reference". Elsevier 8:77-99.

Jacobs PF (1992) Fundamentals in stereolithography, 3D Systems Inc., Valencia, California, USA.

Karalekas DE, Agelopoulos A (2006) On the use of stereolithography built photoelastic models for stress analysis investigations. Materials and Design 27:100-106.

Lantada AD, Sanchez BP, Murillo CG, Sotillo JU (2013) Fractals in tissue engineering: towards biomimetic cell-culture matrices, microsystems and microstructured implants. Expert Rev Med Devic 10(5):1-20.

Lynn-Charney C, Rosen DW (2000) Usage of accuracy models in stereolithography process planning. Rapid Prototyping J 6(2):77-86.

Melchels FP, Feijen J, Grijpma DW (2010) A review on stereolithography and its applications in biomedical engineering. Biomaterials, 31:6121-6130.

Nee AY, Fuh JY, Miyazawa T (2001) On the improvement of the stereolithography (SL) process. J Mater Process Tech 113:262-268.

Ratchev S, Koelemeijer S. (2008) Micro-assembly technologies and applications. Springer.

Richter J, Jacobs PF (1991) The present state of accuracy in stereolithography. Proc. 2nd International Conference on Rapid Prototyping, Dayton, Ohio (USA), 269-294.

Salmoria GV, Ahrens CH, Beal VE, Pires AT, Soldi V (2009) Evalutaion of post-curing and laser manufacturing parameters on the properties of SOMOS 7110 photosensitive resin used in stereolithography. Materials and Design 30:758-763.

Solid Freeform Fabrication Proceedings Symposium, Austin, Texas (USA), 1993.

Varadan VK, Varadan VV (2001) Micro stereo lithography and fabrication of 3D MEMS and their applications. Proc. of SPIE 4952:9-20.

Ventola L, Scaltrito L, Ferrero S, Maccioni G, Chiavazzo E, Asinari P (2014) Micro-structured rough surfaces by laser etching for heat transfer enhancement on flush mounted heat sinks. J. Phys. Conf. S 525:1-10.

Wang WL, Cheah CM, Fuh JY, Lu L (1996) Influence of process parameters on stereolithography part shrinkage. Materials and Design 17(4):205-213.

Zhou J.G, Herschovici D, Chen CC (2000) Parametric process optimization to improve the accuracy of rapid prototyped stereolithography parts. Int. J. Mach. Tool Manu 40:363-379.

Available on-line at: info@funtodo.net